molecular pharmaceutics

Article

Cite This: *Mol. Pharmaceutics* XXXX, XXX, XXX−XXX

pubs.acs.org/molecularpharmaceutics

Short Peptide-Mediated Brain-Targeted Drug Delivery with Enhanced Immunocompatibility

Juan Guan,[†] Zhuxuan Jiang,[†] Mengke Wang,[‡] Ying Liu,[§] Jican Liu,[∥] Yang Yang,[†] Tianhao Ding,[†] Weiyue Lu,[‡] Chunli Gao,*[,⊥] Jun Qian,*[,‡] and Changyou Zhan*[,†,‡]

[†]Department of Pharmacology, School of Basic Medical Sciences & State Key Laboratory of Molecular Engineering of Polymers, Fudan University, Shanghai 200032, P.R. China

[‡]School of Pharmacy, Ministry of Education, Key Laboratory of Smart Drug Delivery, Fudan University, Shanghai 201203, P.R. China

[§]Department of Pathology, School of Basic Medical Sciences, Fudan University, Shanghai 200032, P.R. China

[∥]Department of Pathology, Affiliated Zhongshan Hospital Qingpu Branch, Fudan University, Shanghai 201700, P.R. China

[⊥]Department of Otolaryngology-Head and Neck Surgery, Eye and ENT Hospital, Fudan University, Shanghai 200032, P.R. China

Supporting Information

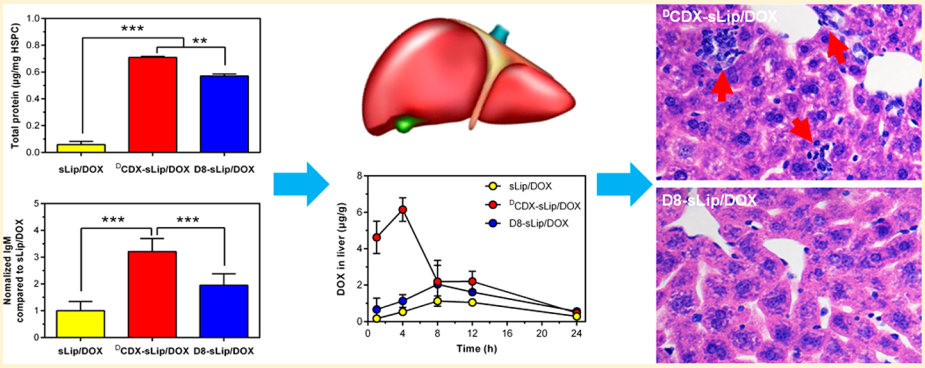

ABSTRACT: Peptide ligands have been exploited as versatile tools to facilitate targeted delivery of nanocarriers. However, the effects of peptide ligands on immunocompatibility and therapeutic efficacy of liposomes remain intricate. Here, a short and stable brain targeted peptide ligand D8 was modified on the surface of doxorubicin-loaded liposomes (D8-sLip/DOX), demonstrating prolonged blood circulation and lower liver distribution in comparison to the long and stable D-peptide ligand ^{D}CDX-modified doxorubicin-loaded liposomes (^{D}CDX-sLip/DOX) by mitigating natural IgM absorption. Despite the improved pharmacokinetic profiles, D8-sLip/DOX exhibited comparable brain targeting capacity in ICR mice and antiglioblastoma efficacy to ^{D}CDX-sLip/DOX in nude mice bearing intracranial glioblastoma. However, dramatic accumulation of ^{D}CDX-sLip/DOX in liver (especially during the first 8 h after intravenous injection) resulted in pathological symptoms, including nuclei swelling, necrosis of liver cells, and inflammation. These results suggest that short peptide ligand-mediated brain-targeted drug delivery systems possessing enhanced immunocompatibility are promising to facilitate efficient brain transport with improved biosafety.

KEYWORDS: *blood−brain barrier, peptide ligand, immunocompatibility, glioblastoma, targeted drug delivery*

INTRODUCTION

Effective delivery of drugs across the blood−brain barrier (BBB) is a major limiting factor in successful therapy of brain disorders.[1−3] The BBB prevents more than 98% of small-molecule drugs and almost 100% of macromolecular therapeutics from entering the brain.[4−6] In addition, the BBB presents a physiological (enzymatic and immunological) barrier to impair brain transport of the majority of therapeutic agents.[7−11] Receptor-mediated transcytosis has been extensively explored to facilitate brain-targeted delivery of macromolecular and nanobased therapeutics.[12,13] Ligand-modified therapeutics in blood circulation recognize corresponding receptors on the brain capillary endothelial cells and initiate receptor-mediated endocytosis. After intracellular transport, those ligand-modified therapeutics can be delivered to the brain side via an exocytosis process. Peptide ligands have been widely exploited to facilitate brain-targeted delivery of nanocarriers.[14−18] After modification on the surface of nanocarriers, those peptide ligands can facilitate brain

Received: November 19, 2018
Revised: January 2, 2019
Accepted: January 8, 2019

DOI: 10.1021/acs.molpharmaceut.8b01216
Mol. Pharmaceutics XXXX, XXX, XXX−XXX

transport via receptor-mediated transcytosis.[19−21] To mitigate enzymatic degradation of peptide ligands in blood circulation and the process of transcytosis (lysosomes are involved in), stable peptide ligands have been developed by cyclization or retro-inverso isomerization techniques in the previous reports.[22,23] The resultant stable peptide ligands improved brain targeting capacity to some extent.[17,24]

Unfortunately, the immunocompatibility of stable peptide ligand-modified nanocarriers has raised many concerns.[25−29] Nicotinic acetylcholine receptors (nAChRs) were found to be highly expressed on the BBB by us and other groups. nAChRs-mediated transcytosis has been successfully exploited to facilitate brain-targeted transport of gene and small-molecule therapeutics.[30,31] ^{D}CDX (G^{D}R^{D}E^{D}I^{D}R^{D}TG^{D}R^{D}A^{D}E^{D}R^{D}W^{D}S^{D}-E^{D}K^{D}F), a 16-mer D-peptide ligand developed by retro-inverso isomerization, is fully resistant to proteolysis in blood circulation and lysosomes of brain capillary endothelial cells.[22] ^{D}CDX improved the brain targeting capacity of its parent L-peptide ligand of nAChRs.[29,32] Our recent study revealed that ^{D}CDX modification played double-edged roles for brain-targeted delivery of liposomes. Stabilization of peptide ligands could maintain bioactivity for receptor binding.[33] While ^{D}CDX-modified liposomes exerted an immune response after absorption of natural IgM on the liposomal surface.

D8 peptide (^{D}RTG^{D}R^{D}A^{D}RE^{D}W) is a rationally designed short peptide that can bind nAChRs with comparable affinity to ^{D}CDX.[34] D8 modification could significantly enhance immunocompatibility of liposomes by lowering natural IgM absorption. However, it remains elusive whether the loading of doxorubicin changes the in vivo performance of D8-modified liposomes. In the present study, the doxorubicin-loaded D8 peptide-modified liposome (D8-sLip/DOX) was prepared, and the benefits from enhanced immunocompatibility were systemically studied. The biodistribution and biosafety of D8-sLip/DOX were assessed in healthy BALB/c mice, and the antiglioblastoma effect was compared with the ^{D}CDX peptide-modified liposomes (^{D}CDX-sLip/DOX) in nude mice bearing intracranial glioblastoma.

MATERIALS AND METHODS

Reagents and Antibodies. HSPC (hydrogenated soy phosphatidylcholine), cholesterol, and mPEG$_{2000}$-DSPE were acquired from A.V.T. (Shanghai) Pharmaceutical Co., Ltd. Fmoc-protected amino acids were purchased from CSBio (Shanghai) Ltd. Mal-PEG$_{3400}$-DSPE was from Laysan Bio Co. (Arab, AL). ^{D}CDX and D8 with an additional cysteine in the N-termini were chemically synthesized using a solid phase peptide synthesizer (CS336, CSBio Ltd.). The fast silver stain kit was from Beyotime Biotechnology (Jiangsu, China). HRP-labeled anti-mouse IgM antibody (ab97230, 1:5000) and anti-CD31 antibody (ab28364, 1:50) were purchased from Abcam (Cambridge, MA).

Animals. Male SD rats, ICR mice, and BALB/c nude mice with an age of 6−8 weeks were purchased from Shanghai SLAC Laboratory Animal Co., Ltd. (Shanghai, China) and kept under SPF condition. All animal experiments were carried out without blinding and in accordance with guidelines evaluated and approved by the ethics committee of Fudan University.

Preparation and Characterization of Doxorubicin-Loaded Liposomes. Doxorubicin loaded liposomes, including plain liposomes (sLip/DOX), ^{D}CDX peptide-modified liposomes (^{D}CDX-sLip/DOX), and D8 peptide-modified liposomes (D8-sLip/DOX) were prepared according to previous reports (the conjugation chemistry is shown in Figure S1).[22] A mixture of lipids (mPEG$_{2000}$-DSPE/cholesterol/HSPC 5/45/50, ^{D}CDX-PEG$_{3400}$-DSPE/mPEG$_{2000}$-DSPE/cholesterol/HSPC 2/3/45/50, or D8-PEG$_{3400}$-DSPE/mPEG$_{2000}$-DSPE, 2/3/45/50) in $CHCl_3$ was rotary evaporated to form a thin film. Any residual $CHCl_3$ was removed by evaporation under vacuum. The thin film was hydrated with 0.32 M $(NH_4)_2SO_4$ and extruded through polycarbonate membranes with a pore size of 400, 200, and 100 nm. Unencapsulated $(NH_4)_2SO_4$ was replaced by saline using a Sephadex G-50 column. Doxorubicin was loaded at a mass ratio of 1:10 to lipids, vibrating for 20 min at 60 °C. Any unencapsulated doxorubicin was removed by a Sephadex G-50 column.

The size and zeta potential of liposomes were detected using Zetasizer Nano ZS90. The encapsulation efficiency and loading capacity of doxorubicin in liposomes were measured by dissolving the freeze-dried liposomes in 5% Triton X-100, and the content of doxorubicin was quantified by a microplate reader at 480 nm. Drug loading (DL) and encapsulation efficiency (EE) were calculated as DL(%) = weight of drug/weight of liposomes ×100% and EE(%) = measured drug content/drug feeding content ×100%.

Separation and Characterization of Protein Coronas. Doxorubicin-loaded liposomes (100 μL) were mixed with an equal volume of serum and incubated at 37 °C for 1 h. Cold PBS (800 μL) was added, and the samples were centrifuged (14 000*g*) for 30 min at 4 °C. The deposit was rinsed thrice with cold PBS and resuspended in 25 μL of PBS.

The total amount of proteins was measured using the BCA kit according to the manufacturer's instructions. To analyze the composition of protein coronas, protein corona suspensions were mixed with β-mercaptoethanol (2 μL) and loading buffer (6.5 μL) and boiled for 5 min. The proteins were separated by 4−20% SDS-PAGE and stained with a silver staining kit. For nano-LC−MS/MS identification, the entire gel was cut into pieces and destined, reduced, and alkylated, followed by trypsin digestion. The digested peptides were extracted and analyzed by an LTQ Orbitrap Fusion mass spectrometer (Thermo Electron, San Jose, CA). Data were analyzed as previously reported.[13] For Western-blotting, the gel was transferred to the PVDF membrane, and natural IgM was detected using goat anti-mouse IgM antibody conjugated with HRP.

Biodistribution of DOX in Mice. Male ICR mice (20−25 g, n = 5) were divided into 4 groups and treated with saline, sLip/DOX, ^{D}CDX-sLip/DOX, and D8-sLip/DOX at a doxorubicin dose of 2 mg/kg. After blood sampling, mice were perfused with saline, and the main organs were dissected and stored at −20 °C for use. All organs were weighed, and 10% (w/v) distilled water was added. After being smashed, 200 μL of homogenates was sampled and successively mixed with 50 μL of daunorubicin hydrochloride solution (10 μg/mL, internal standard), 400 μL of chloroform, and 100 μL of methanol. After being vortexed and mixed for 1 min, the mixture was centrifuged (10 000*g*) for 5 min, and the chloroform layer was separated and dried at room temperature. The samples were reconstituted in 100 μL of methanol, and doxorubicin was quantified using HPLC with a fluorescence detector at 480 nm/550 nm.

DOI: 10.1021/acs.molpharmaceut.8b01216
Mol. Pharmaceutics XXXX, XXX, XXX−XXX

Table 1. Characterization of Doxorubicin-Loaded Liposomes[a]

	size (nm)	PDI	zeta potential (mV)	DL (%)	EE (%)
sLip/DOX	117.0 ± 1.62	0.037 ± 0.02	−16.4 ± 0.59	5.23	96.88
^{D}CDX-sLip/DOX	125.3 ± 0.85	0.070 ± 0.01	−7.79 ± 0.26	4.90	97.66
D8-sLip/DOX	122.9 ± 1.24	0.039 ± 0.03	−8.23 ± 0.15	5.04	99.21

[a]DL, drug loading efficiency, and EE, encapsulation efficiency.

Biosafety Evaluation of DOX-Loaded Liposomes. Biosafety evaluation was carried out in male ICR mice (20−25 g, n = 5). Mice were divided into four groups and treated with saline, sLip/DOX, ^{D}CDX-sLip/DOX, and D8-sLip/DOX at a total doxorubicin dose of 12 mg/kg (6 injections, every 3 days). After treatment, blood was sampled, and the main organs were dissected, immersed in 4% PFA for 24 h, dehydrated, and embraced in paraffin. Sectioned slices were stained with hematoxylin and eosin and visualized using a microscope. AST/GOT (glutamic oxalacetic transaminase), ALT/GPT (glutamic-pyruvic transaminase), AKP (alkline phosphatase), creatine kinase, BUN (blood urea nitrogen), and CRE (serum creatinine) were measured using the standard assay kits.

Brain Targeting Efficiency in Vivo. To study the brain targeting ability, ICR mice were injected with sLip/DOX, ^{D}CDX-sLip/DOX, and D8-sLi/DOX liposomes at a doxorubicin dose of 2 mg/kg. Mice were anesthetized and perfused with saline and 4% PFA successively at 4 and 8 h after injection of liposomes. Brains were dissected and immersed in 4% PFA for 24 h, then dehydrated with 30% sucrose solution, and embedded in OCT for sectioning. The slices were stained with rabbit anti-mouse CD31 antibody and FITC-conjugated goat anti-rabbit IgG.

Cytotoxicity Assay. U87 cells lines (1500 cells/well) were seeded in a 96-well plate with 100 μL of medium. After 24 h, different doxorubicin formulations (100 μL, free doxorubicin, sLip/DOX, ^{D}CDX-sLip/DOX, and D8-sLip/DOX) were added. After 96 h, MTS solution was added to each well, and the absorbance at 429 nm was detected to calculate cell viability.

Antiglioma Effect in Vivo. BALB/c nude mice bearing intracranial glioblastoma were constructed as described in previous reports.[13] The model mice were divided into five groups (n = 12) and treated with saline, free doxorubicin, sLip/DOX, ^{D}CDX-sLip/DOX, and D8-sLip/DOX via tail vein at a total doxorubicin dose of 10 mg/kg (at day 7, 9, 11, 13, and 15 after glioblastoma cells implantation). Body weight and the survival time were recorded.

Statistical Analysis. Data were presented as means ± standard deviations (SD) and analyzed by Student's t-test using GraphPad Prism software. $p < 0.05$ was considered statistically significant.

RESULTS AND DISCUSSION

Characterization of Doxorubicin-Loaded Liposomes. Doxorubicin-loaded plain liposomes (sLip/DOX), ^{D}CDX-modified liposomes (^{D}CDX-sLip/DOX), and D8-modified liposomes (D8-sLip/DOX) were prepared using an ammonium sulfate gradient loading technique as previously reported (see the Methods section) and stored in saline.[22] The size and zeta-potential of liposomes were characterized by dynamic light scattering (Table 1). sLip/DOX, ^{D}CDX-sLip/DOX, and D8-sLip/DOX exhibited comparable diameters of 120 nm. The zeta potential of plain liposomes was −16 mV. Modification of both peptide ligands could significantly increase zeta-potential of liposomes to −8 mV, which may attribute to the positively charged amino acids in both ^{D}CDX and D8 (see peptide sequences in Table S1).

The loading capacity and encapsulation efficiency of doxorubicin in liposomes were measured using a microplate reader (see the Methods section). As shown in Table 1, doxorubicin displayed high encapsulation efficiency in all populations of liposomes (>96%), and the loading capacities were around 5%. Modification of neither ^{D}CDX nor D8 affected drug loading.

Characterization of Protein Coronas. To analyze the composition of protein coronas, sLip/DOX, ^{D}CDX-sLip/DOX, and D8-sLip/DOX were incubated with mouse serum in vitro at 37 °C for 1 h. The formed protein coronas were collected by centrifugation and rinsed with cold PBS to remove unassociated plasma proteins. The total amount of bound plasma proteins was measured using BCA kits. As shown in Figure 1a, both ^{D}CDX and D8 peptide modification

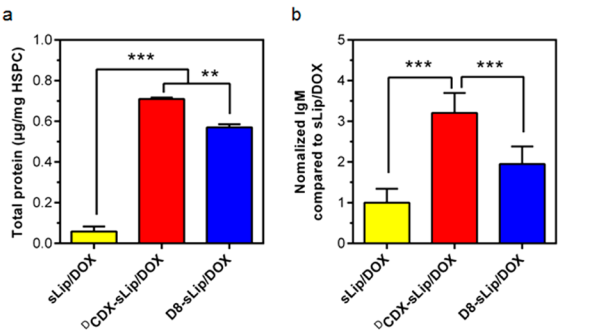

Figure 1. Protein corona formed on the surface of sLip/DOX, ^{D}CDX-sLip/DOX, and D8-sLip/DOX after incubation with mouse serum at 37 °C for 1 h. (a) The total amount of absorbed protein liposomal surface. (b) Normalization of natural IgM absorbed on liposomal surface. Data are means ± SD (n = 3).

significantly increased the absorption of plasma proteins on liposomal surface. The absorbed plasma proteins were further characterized using SDS-PAGE (Figure S2a). Modification of ^{D}CDX peptide ligands resulted in a significant increase of a protein band at 72 kDa, which was ascertained as natural IgM by nano-LC−MS/MS. It was consistent with our previous report,[25] in which natural IgM was found to preferably bind ^{D}CDX-modified blank liposomes (also confirmed in Figure S2a). This result suggested that doxorubicin loading did not significantly change the composition of the formed protein corona on liposomal surface. As quantified using Western-blotting (Figure S2b), ^{D}CDX-sLip absorbed a 3-fold higher amount of natural IgM than sLip/DOX did. Whereas D8-sLip/DOX absorbed less than 2-fold compare to sLip/DOX. The compositions of formed protein coronas were ascertained using nano-LC−MS/MS. Modification of both ^{D}CDX and D8 dramatically increased the number of detectable plasma

DOI: 10.1021/acs.molpharmaceut.8b01216
Mol. Pharmaceutics XXXX, XXX, XXX−XXX

proteins in comparison to sLip/DOX (Figure 2a), while it relatively decreased the ratio of plasma proteins of 40−50 kDa molecular weight (Figure 2b) and of 5−6 isoelectric point (Figure 2c).

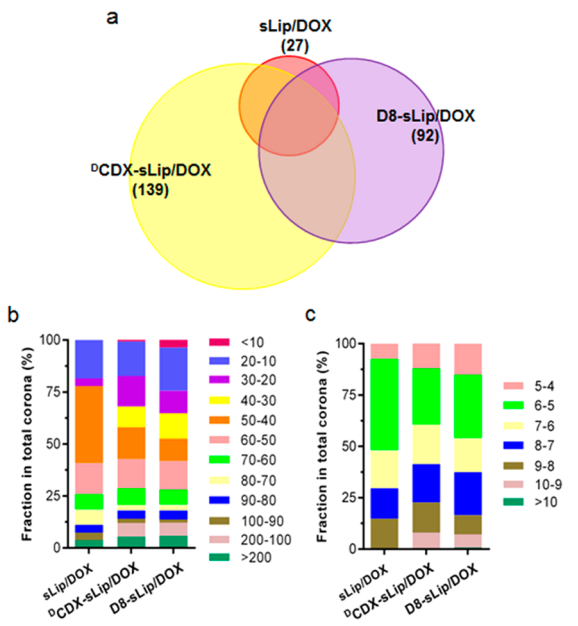

Figure 2. Characterization of protein coronas on liposomal surface. (a) The number of detectable plasma proteins and category based on (b) molecular weight and (c) isoelectric point.

Natural IgM Absorption Accelerates Clearance of Doxorubicin-Loaded Liposomes. To investigate whether natural IgM absorption could accelerate clearance of doxorubicin-loaded liposomes, the pharmacokinetic profiles of sLip/DOX, DCDX-sLip/DOX, and D8-sLip/DOX were studied in ICR mice (Figure 3a) and SD rats (Figure 3b). As

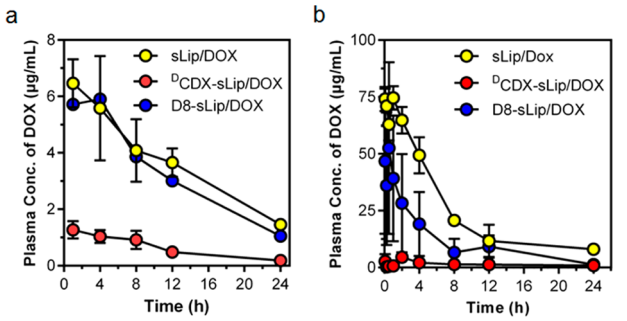

Figure 3. Pharmacokinetic profiles of liposomes in ICR mice (a) and SD rats (b). Data are means ± SD (n = 4).

expected, sLip/DOX showed prolonged circulation in both mice and rats; while modification of DCDX on liposomal surface extremely accelerated blood clearance of encapsulated doxorubicin in comparison to sLip/DOX (Table 2). Modification of D8 could significantly mitigate accelerated clearance of encapsulated doxorubicin. In previous reports, PEGylated liposomes demonstrated strong accelerated blood clearance (ABC) phenomena after preadministration of a small dose of blank liposomes (5−7 days before).[35,36] The B lymphocytes and the acquired anti-PEG IgM plays important roles in the occurrence of ABC phenomena,[37] and the loading of cytotoxic payloads (e.g., doxorubicin) can dramatically mitigate the ABC phenomena.[38] In comparison to the ABC phenomena, accelerated clearance of DCDX-sLip/DOX may result in more profound influence on the performance of liposomes, since natural IgM exerts many functions in the innate immune system. Thus, the acquired D8 peptide would be a promising brain targeting ligand to improve immunocompatibility of liposomes.

Enhanced Accumulation of DCDX-sLip/DOX Induces Liver Disorders. To detect the in vivo fate of liposomes, ICR mice were injected with sLip/DOX, DCDX-sLip/DOX, and D8-sLip/DOX via tail vein at a doxorubicin dose of 2 mg/kg. Mice were anesthetized and sacrificed at the predetermined time points. The main organs were dissected, and the biodistribution of doxorubicin after treatments of different populations of liposomes were measured. As shown in Figure 4a, doxorubicin exhibited a dramatic accumulation in the liver

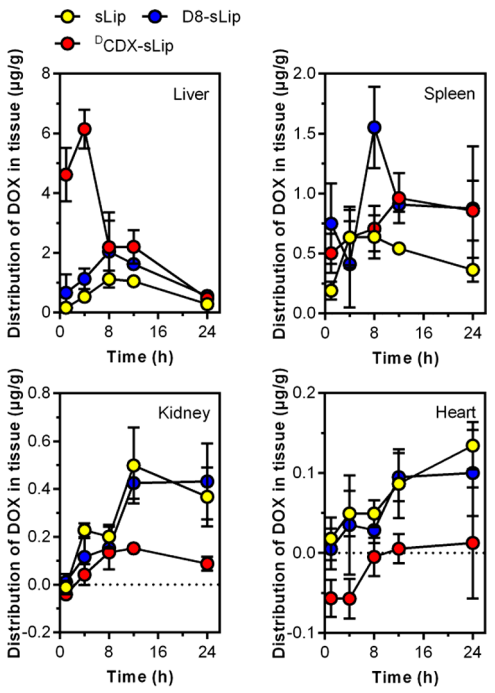

Figure 4. Biodistribution of sLip/DOX, DCDX-sLip/DOX, and D8-sLip/DOX in the main organ of ICR mice. Data are means ± SD (n = 4).

Table 2. Area under the Pharmacokinetic Curve (AUC) Calculated by GraphPad Prism 6.0 (n = 4)

	mouse			rat		
liposomes	sLip/DOX	DCDX-sLip/DOX	D8-sLip/DOX	sLip/DOX	DCDX-sLip/DOX	D8-sLip/DOX
AUC (μg/mL h)	87.2	14.2	69.7	570.4	47.76	313.5
SD	9.6	0.4	4.6	123.1	16.46	115.8

DOI: 10.1021/acs.molpharmaceut.8b01216
Mol. Pharmaceutics XXXX, XXX, XXX−XXX

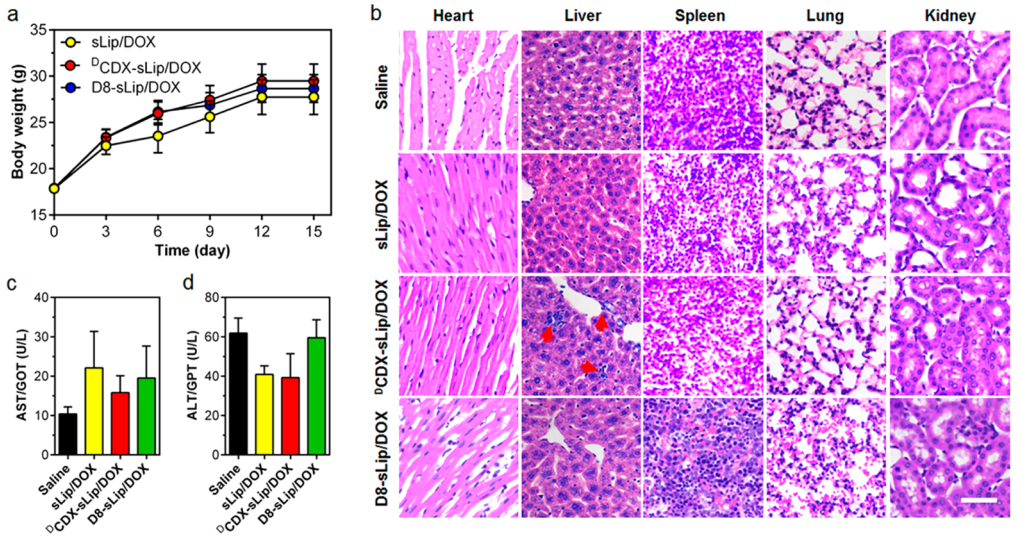

Figure 5. Biosafety evaluation of sLip/DOX, ^{D}CDX-sLip/DOX, and D8-sLip/DOX in ICR mice. (a) Body weight change of ICR mice after treatment with doxorubicin-loaded liposomes. (b) Microscopic observation of H&E stained slice of main organs after treatments of liposomes (scale bar = 50 μm). Red arrows indicate inflammatory cell infiltration. The plasma level of AST/GOT (c) and ALT/GPT (d) in ICR mice after treatments of liposomes. Data are means ± SD (n = 5).

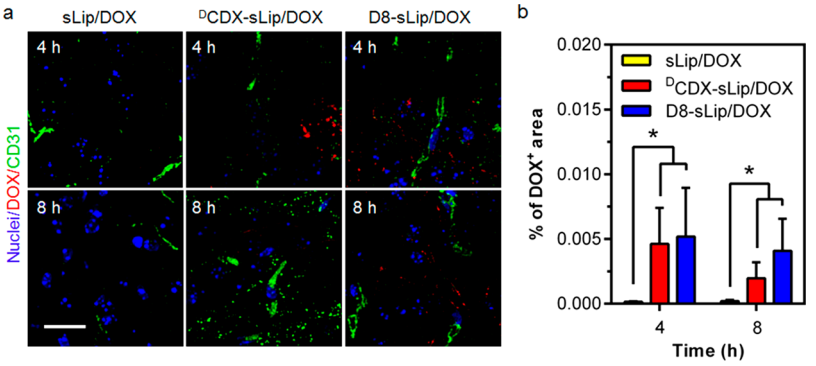

Figure 6. Biodistribution of doxorubicin in the cerebral cortex of ICR mice at 4 and 8 h. (a) Microscopic observation of frozen section of brains stained with anti-CD31 antibody (green) and DAPI (blue) after treatment of doxorubicin (red)-loaded liposomes using a confocal laser scanning microscope. (b) Semiquantitation of doxorubicin in brain based on fluorescence by Image Pro. Data are means ± SD (n = 4).

about 5−7-fold at 1 and 4 h after injection of ^{D}CDX-sLip/DOX in comparison to sLip/DOX and D8-sLip/DOX; while such enhanced accumulation disappeared after 8 h. There was no significant difference of DOX accumulation in spleen among sLip/DOX, ^{D}CDX-sLip/DOX, and D8-sLip/DOX (Figure 4b). Meanwhile, DOX accumulation in kidney (Figure 4c) and heart (Figure 4d) in ^{D}CDX-dsLip/DOX-treated mice was slightly lower than that in sLip/DOX and D8-sLip/DOX-treated mice, which may be due to the accumulation of ^{D}CDX-sLip/DOX in liver (Figure 4a).

To assess the biosafety profiles of different populations of liposomes, ICR mice were divided into 4 groups and received 6 injections (every 3 days) of saline, sLip/DOX, ^{D}CDX-sLip/DOX, or D8-sLip/DOX at a total doxorubicin dose of 12 mg/kg. After treatments, the body weights of all mice treated with liposomes did not exhibit a significant difference (Figure 5a), indicating that none of those populations of doxorubicin-loaded liposomes could exert obvious toxicity. All organs were dissected and subject to hematoxylin and eosin (H&E) staining (Figure 5b). No evidence of toxicity in heart, spleen, and kidney was found in all of the doxorubicin-loaded liposome-treated mice. All the sections in the slices of kidney showed normal glomeruli and tubules. The cardiac muscles and endometrial were healthy, which was consistent with the previous reports that liposome formulation could significantly mitigate the myocardial toxicity of free doxorubicin.[39−41]

The ALT/GPT and AST/GOT levels in plasma were measured, and the results are shown in Figure 5c,d, indicating that doxorubicin-loaded liposomes did not significantly affect the liver functions. However, the livers of ^{D}CDX-sLip/DOX-treated mice exhibit some pathological features. Fatty hepatocytes were found in one mouse after ^{D}CDX-sLip/DOX treatment, and the nuclei were swollen, and the liver cells were dissolved due to putrescence (Figure S3). In the other three mice treated with ^{D}CDX-sLip/DOX, inflammatory cell infiltration was found in the livers (Figure 5b). Even though this only happened in several cells rather than in a wide range, future applications of ^{D}CDX-sLip/DOX might be cautious, particularly when repeated treatments are needed.

Brain Targeting Capacity of Peptide-Modified Liposomes. To evaluate the brain targeting capacity, ICR mice were intravenously injected with sLip/DOX, ^{D}CDX-sLip/DOX, or D8-sLip/DOX at a doxorubicin dose of 2 mg/kg via tail vein. Mice were euthanized at 4 and 8 h after treatment,

DOI: 10.1021/acs.molpharmaceut.8b01216
Mol. Pharmaceutics XXXX, XXX, XXX−XXX

and the whole brains were dissected for frozen sectioning. The blood vessels in cerebrum were labeled with anti-CD31 antibody, and brain distribution of doxorubicin was semi-quantified by fluorescence. As shown in Figure 6, ^{D}CDX-sLip/DOX and D8-sLip/DOX groups displayed a higher distribution in the cerebral cortex at both time points after injection than sLip/DOX. sLip/DOX had nearly no distribution in the brain. At 8 h after injection, the brain distribution of ^{D}CDX-sLip/DOX slightly decreased compared to that at 4 h after injection, while D8-sLip/DOX remained a comparable brain distribution to that at 4 h. These results indicated that both ^{D}CDX and D8 peptide could facilitate the liposomes across the BBB in vivo, and D8-sLip/DOX could maintain a relatively longer duration than ^{D}CDX-sLip/DOX, which may attribute to the slower blood clearance of D8-sLip/DOX.

Antiglioblastoma Effect. To evaluate the in vitro antiglioma effect, U87 cells were incubated with different doxorubicin formulations (free doxorubicin, sLip/DOX, ^{D}CDX-sLip/DOX, and D8-sLip/DOX) for 96 h. The cell viability was measured using MTS. As shown in Figure S4, both sLip/DOX and D8-sLip/DOX demonstrated comparable antiglioblastoma effect to free doxorubicin. However, ^{D}CDX modification enhanced the in vitro antiglioblastoma effect of doxorubicin by 4-fold.

To evaluate the therapeutic efficiency in vivo, nude mice bearing intracranial U87 cells received saline, free doxorubicin, sLip/DOX, ^{D}CDX-sLip/DOX, and D8-sLip/DOX at a doxorubicin dose of 2 mg/kg via tail vein at the seventh, ninth, 11th, 13th, and 15th day after glioblastoma implantation. As shown in Figure 7, free doxorubicin (p = 0.0008 vs saline group) and sLip/DOX (p = 0.0067 vs saline group) could slightly prolong the median survival time of model mice from 19 days (saline group) to 22.5 days. Modification of peptide ligands could further lengthen the survival time of model mice to 25.5 days (^{D}CDX-sLip/DOX, $p < 0.0001$ vs saline group) or 26 days (D8-sLip/DOX, $p < 0.0001$ vs saline group), indicating that enhanced brain permeability of doxorubicin-loaded liposomes could improve the antiglioblastoma effect. D8-sLip/DOX did not show advantages in prolonging the survival time of model mice over ^{D}CDX-sLip/DOX.

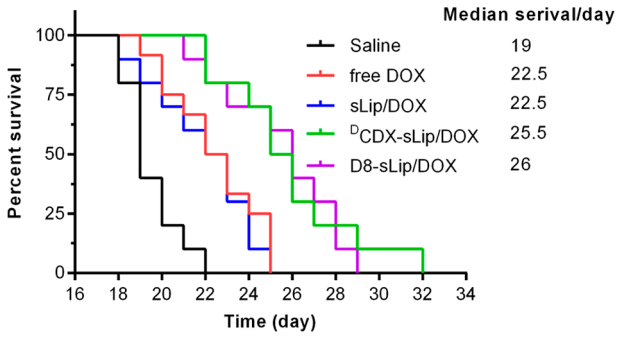

Figure 7. Kaplan–Meier survival curve of nude mice bearing intracranial U87 glioma after treatment of saline (black, 19 days, n = 9), free DOX (red, 22.5 days, n = 10), sLip/DOX (blue, 22.5 days, n = 9), ^{D}CDX-sLip/DOX (green, 25.5 days, n = 10), and D8-sLip/DOX (purple, 26 days, n = 10) at a total DOX dose of 10 mg/kg (injections at day 7, 9, 11, 13, and 15 after glioma implantation). Data were plotted, and the median survival time was calculated using GraphPad Prism 6.0.

CONCLUSION

D8 peptide was a rationally designed brain targeting ligand based on the mechanistic understanding of ^{D}CDX peptide-mediated brain-targeted liposomes. The immunocompatibility of D8-modified liposomes was improved by mitigating natural IgM absorption, which could cause recognition of drug delivery systems by mononuclear phagocytic systems. In the present study, encapsulation of doxorubicin did not change the pharmacokinetics of liposomes. Prolonged circulation of D8-sLip/DOX did not significantly improve the brain targeting efficiency and antiglioblastoma effect in comparison to ^{D}CDX-sLip/DOX, while a decrease of accumulation in liver during the first 8 h after intravenous injection makes D8-sLip/DOX a better brain-targeted formulation for high biosafety.

ASSOCIATED CONTENT

Supporting Information

The Supporting Information is available free of charge on the ACS Publications website at DOI: 10.1021/acs.molpharmaceut.8b01216.

Scheme of the chemical synthesis of peptide-conjugated PEG3400-DSPE, protein corona characterization, microscopic observation of liver slices, cytotoxicity assay, and peptide sequence (PDF)

AUTHOR INFORMATION

Corresponding Authors

*E-mail: elvasunny@163.com.
*E-mail: qianjun@fudan.edu.cn.
*Tel: 86-21-54237379; E-mail: cyzhan@fudan.edu.cn.

ORCID

Juan Guan: 0000-0002-5944-6512
Yang Yang: 0000-0001-5444-7535
Weiyue Lu: 0000-0001-8003-2675

Notes

The authors declare no competing financial interest.

ACKNOWLEDGMENTS

This work was supported by the National Natural Science Foundation of China (81673361, 81690263, 81803455 and 81673370), Shanghai Education Commission Major Project (2017-01-07-00-07-E00052), Shanghai Natural Science Foundation (18ZR1404800), and Shanghai Municipal Health Commission (2018BR04).

REFERENCES

(1) Vlieghe, P.; Khrestchatisky, M. Peptide-based vectors for blood-brain barrier targeting and delivery of drugs to the central nervous system. *Ther. Delivery* **2010**, *1* (4), 489–94.
(2) Georgieva, J. V.; Hoekstra, D.; Zuhorn, I. S. Smuggling Drugs into the Brain: An Overview of Ligands Targeting Transcytosis for Drug Delivery across the Blood-Brain Barrier. *Pharmaceutics* **2014**, *6* (4), 557–83.
(3) Simionescu, M.; Popov, D.; Sima, A. Endothelial transcytosis in health and disease. *Cell Tissue Res.* **2009**, *335* (1), 27–40.
(4) Pardridge, W. M. Blood-brain barrier drug targeting: the future of brain drug development. *Mol. Interventions* **2003**, *3* (2), 90–105 51 .
(5) Gao, H. Progress and perspectives on targeting nanoparticles for brain drug delivery. *Acta Pharm. Sin. B* **2016**, *6* (4), 268–86.
(6) He, Q.; Liu, J.; Liang, J.; Liu, X.; Li, W.; Liu, Z.; Ding, Z.; Tuo, D. Towards Improvements for Penetrating the Blood-Brain Barrier-

DOI: 10.1021/acs.molpharmaceut.8b01216
Mol. Pharmaceutics XXXX, XXX, XXX–XXX

Recent Progress from a Material and Pharmaceutical Perspective. *Cells* **2018**, *7* (4), 24.
(7) Wekerle, H. Immune protection of the brain—efficient and delicate. *J. Infect. Dis.* **2002**, *186*, S140—4.
(8) Muldoon, L. L.; et al. Immunologic privilege in the central nervous system and the blood-brain barrier. *J. Cereb. Blood Flow Metab.* **2013**, *33* (1), 13—21.
(9) Stolp, H. B.; Liddelow, S. A.; Sá-Pereira, I.; Dziegielewska, K. M.; Saunders, N. R. Immune responses at brain barriers and implications for brain development and neurological function in later life. *Front. Integr. Neurosci.* **2013**, *7*, 61.
(10) Mauro, C.; De Rosa, V.; Marelli-Berg, F.; Solito, E. Metabolic syndrome and the immunological affair with the blood-brain barrier. *Front. Immunol.* **2015**, *5*, 677.
(11) Pachter, J. S.; de Vries, H. E.; Fabry, Z. The blood-brain barrier and its role in immune privilege in the central nervous system. *J. Neuropathol. Exp. Neurol.* **2003**, *62* (6), 593—604.
(12) Dong, X. Current Strategies for Brain Drug Delivery. *Theranostics* **2018**, *8* (6), 1481—1493.
(13) Guan, J.; Zhang, Z.; Hu, X.; Yang, Y.; Chai, Z.; Liu, X.; Liu, J.; Gao, B.; Lu, W.; Qian, J.; Zhan, C. Cholera Toxin Subunit B Enabled Multifunctional Glioma-Targeted Drug Delivery. *Adv. Healthcare Mater.* **2017**, *6* (23), 1700709.
(14) Demeule, M.; et al. Identification and design of peptides as a new drug delivery system for the brain. *J. Pharmacol. Exp. Ther.* **2007**, *324* (3), 1064—72.
(15) Demeule, M.; et al. Involvement of the low-density lipoprotein receptor-related protein in the transcytosis of the brain delivery vector angiopep-2. *J. Neurochem.* **2008**, *106* (4), 1534—44.
(16) Regina, A.; et al. Antitumour activity of ANG1005, a conjugate between paclitaxel and the new brain delivery vector Angiopep-2. *Br. J. Pharmacol.* **2008**, *155* (2), 185—97.
(17) Taylor, E. M.; Otero, D. A.; Banks, W. A.; O'Brien, J. S. Retro-inverso prosaptide peptides retain bioactivity, are stable In vivo, and are blood-brain barrier permeable. *J. Pharmacol Exp Ther* **2000**, *295* (1), 190—194.
(18) Wei, X.; et al. Retro-inverso isomer of Angiopep-2: a stable d-peptide ligand inspires brain-targeted drug delivery. *Mol. Pharmaceutics* **2014**, *11* (10), 3261—8.
(19) Vieira, D. B.; Gamarra, L. F. Getting into the brain: liposome-based strategies for effective drug delivery across the blood-brain barrier. *Int. J. Nanomed.* **2016**, *11*, 5381—5414.
(20) Johnsen, K. B.; Burkhart, A.; Melander, F.; Kempen, P. J.; Vejlebo, J. B.; Siupka, P.; Nielsen, M. S.; Andresen, T. L.; Moos, T. Targeting transferrin receptors at the blood-brain barrier improves the uptake of immunoliposomes and subsequent cargo transport into the brain parenchyma. *Sci. Rep.* **2017**, *7* (1), 10396.
(21) Lam, F. C.; Morton, S. W.; Wyckoff, J.; Vu Han, T.-L.; Hwang, M. K.; Maffa, A.; Balkanska-Sinclair, E.; Yaffe, M. B.; Floyd, S. R.; Hammond, P. T. Enhanced efficacy of combined Temozolomide and bromodomain inhibitor therapy for gliomas using targeted nanoparticles. *Nat. Commun.* **2018**, *9* (1), 1991.
(22) Wei, X.; et al. A D-peptide ligand of nicotine acetylcholine receptors for brain-targeted drug delivery. *Angew. Chem., Int. Ed.* **2015**, *54* (10), 3023—7.
(23) Wang, R.; et al. Efficacy of inverso isomer of CendR peptide on tumor tissue penetration. *Acta Pharm. Sin. B* **2018**, *8* (5), 825—832.
(24) Oller-Salvia, B.; et al. Blood-brain barrier shuttle peptides: an emerging paradigm for brain delivery. *Chem. Soc. Rev.* **2016**, *45* (17), 4690—707.
(25) Guan, J.; Shen, Q.; Zhang, Z.; Jiang, Z.; Yang, Y.; Lou, M.; Qian, J.; Lu, W.; Zhan, C. Enhanced immunocompatibility of ligand-targeted liposomes by attenuating natural IgM absorption. *Nat. Commun.* **2018**, *9* (1), 2982.
(26) Allen, T. M.; Cullis, P. R. Drug delivery systems: entering the mainstream. *Science* **2004**, *303* (5665), 1818—22.
(27) Bae, Y. H.; Park, K. Targeted drug delivery to tumors: myths, reality and possibility. *J. Controlled Release* **2011**, *153* (3), 198—205.
(28) Nag, O. K.; et al. Liposomes modified with superhydrophilic polymer linked to a nonphospholipid anchor exhibit reduced complement activation and enhanced circulation. *J. Pharm. Sci.* **2015**, *104* (1), 114—23.
(29) Nag, O. K.; Awasthi, V. Surface engineering of liposomes for stealth behavior. *Pharmaceutics* **2013**, *5* (4), 542—69.
(30) Chen, W.; et al. Targeted brain delivery of itraconazole via RVG29 anchored nanoparticles. *J. Drug Target* **2011**, *19* (3), 228—34.
(31) Fu, C.; et al. Targeted transport of nanocarriers into brain for theranosis with rabies virus glycoprotein-derived peptide. *Mater. Sci. Eng., C* **2018**, *87*, 155—166.
(32) Zhan, C.; et al. Micelle-based brain-targeted drug delivery enabled by a nicotine acetylcholine receptor ligand. *Angew. Chem., Int. Ed.* **2011**, *50* (24), 5482—5.
(33) Vlieghe, P.; et al. Synthetic therapeutic peptides: science and market. *Drug Discovery Today* **2010**, *15* (1—2), 40—56.
(34) Ying, M.; et al. Liposome-Based Systemic Glioma-Targeted Drug Delivery Enabled by All-d Peptides. *ACS Appl. Mater. Interfaces* **2016**, *8* (44), 29977—29985.
(35) Ishida, T.; et al. Spleen plays an important role in the induction of accelerated blood clearance of PEGylated liposomes. *J. Controlled Release* **2006**, *115* (3), 243—50.
(36) Wang, X.; Ishida, T.; Kiwada, H. Anti-PEG IgM elicited by injection of liposomes is involved in the enhanced blood clearance of a subsequent dose of PEGylated liposomes. *J. Controlled Release* **2007**, *119* (2), 236—44.
(37) Shimizu, T.; et al. Anti-PEG IgM and complement system are required for the association of second doses of PEGylated liposomes with splenic marginal zone B cells. *Immunobiology* **2015**, *220* (10), 1151—60.
(38) Callaghan, R.; Luk, F.; Bebawy, M. *Drug Metab. Dispos.* **2014**, *42* (4), 623—31.
(39) Ding, Y.; et al. In vivo study of doxorubicin-loaded cell-penetrating peptide-modified pH-sensitive liposomes: biocompatibility, bio-distribution, and pharmacodynamics in BALB/c nude mice bearing human breast tumors. *Drug Des., Dev. Ther.* **2017**, *11*, 3105—3117.
(40) Koren, E.; et al. Multifunctional PEGylated 2C5-immunoliposomes containing pH-sensitive bonds and TAT peptide for enhanced tumor cell internalization and cytotoxicity. *J. Controlled Release* **2012**, *160* (2), 264—73.
(41) Kale, A. A.; Torchilin, V. P. "Smart" drug carriers: PEGylated TATp-modified pH-sensitive liposomes. *J. Liposome Res.* **2007**, *17* (3—4), 197—203.

DOI: 10.1021/acs.molpharmaceut.8b01216
Mol. Pharmaceutics XXXX, XXX, XXX—XXX